FRF Measurements Subject to Missing Data: Quantification of Noise, Nonlinear Distortion, and Time-Varying Effects

Pintelon, Rik; Lataire, John; Vandersteen, Gerd

Published in:
IEEE Transactions on Instrumentation and Measurement

DOI:
10.1109/TIM.2018.2883998

Publication date:
2019

Document Version:
Submitted manuscript

FRF Measurements Subject to Missing Data: Quantification of Noise, Nonlinear Distortion, and Time-Varying Effects

Rik Pintelon, John Lataire, and Gerd Vandersteen
Vrije Universiteit Brussel, department ELEC, Pleinlaan 2, 1050 Brussel, Belgium (email: Rik.Pintelon@vub.ac.be)

***Abstract*—Quantifying the level of nonlinear distortions and time-varying effects in frequency response function (FRF) measurements is a first step towards the selection of an appropriate parametric model structure. In this paper we tackle this problem in the presence of missing data, which is an important issue in large-scale low-cost wireless sensor networks. The proposed method is based on one experiment with a special class of periodic excitation signals.**

***Index Terms*—frequency response function (FRF), time-varying frequency response function (TV-FRF), nonparametric estimates, nonlinear distortion, time-varying systems, random phase multisine**

I. Introduction

In many scientific disciplines parametric models are identified from experiments on dynamical systems either to get insight into complex physical phenomena, or for computer aided design, fault detection/monitoring, prediction and control [1]. Choosing the appropriate model structure of the parametric model is one of the most difficult steps in the identification procedure. A nonparametric procedure allowing the user/scientist to decide which type of dynamical model structure is most appropriate for a particular application would be very helpful in this respect.

A first step towards the solution of this difficult problem is presented in [2]: via an experiment with a random phase multisine, which is a special periodic signal (see Section II-B for a precise definition), the time-varying frequency response function (TV-FRF, see Section II-A for a precise definition), the noise level, the level of nonlinear distortions and the time-varying effects are estimated nonparametrically. It allows one to decide which of the following dynamical models is best suited to describe the measurements: linear time-invariant (LTI), linear time-varying (LTV), nonlinear time-invariant (NLTI), or nonlinear time-varying (NLTV). In addition, it gives insight into the complexity of LTI and LTV dynamics via the best linear time-invariant and best linear time-varying approximations, respectively.

In this paper we extend the results of [2] to measurements subject to missing data. The proposed approach is based on a non-trivial combination of the algorithm for estimating the time-varying frequency response function using random phase multisines [2] and the missing data algorithm for frequency response functions using periodic excitations [3].

The time-variation of the dynamics can be smooth and non-periodic (e.g. thermal drift in high frequency power amplifiers [4], and fatigue in bio-medical experiments [5]), smooth and periodic (e.g. lung acoustical impedance measurement [6], and rotating machines [7]), and non-smooth (e.g. switched [8] and hybrid [9] systems). This paper considers only smooth nonperiodic time-varying dynamics.

Missing data are due to data loss in wireless transmission and/or sensor malfunction (e.g. clipping and outliers result in wrong measurements that should be removed), and is an issue in large-scale low-cost wireless sensor networks [10]. To save transmission power and communication resources data can be intentionally discarded and transmission errors as high as 30% are possible for wireless communication platforms [11]. Hence, in some measurement applications missing data are an important issue, and in this paper we handle the impact of missing data on the nonparametric estimation of the TV-FRF, the noise level and the level of nonlinear distortions.

Very few results are available in the literature on the identification of time-varying systems in the presence of missing data: [12] states that the parametric maximum likelihood solution for LTI systems can be extended to time-varying discrete-time models, and [13] mentions that the parametric algorithm for autonomous periodically time-varying systems is also applicable in case of missing data. While the parametric maximum likelihood approaches [12], [14] cannot handle missing data patterns that depend on the signal (e.g. clipping), the nonparametric method presented in this paper imposes no condition on the missing data pattern except that samples missing at the borders of the excitation periods are excluded. In addition, none of these parametric techniques can detect and quantify the level of the nonlinear distortions. The latter is also valid for the nonparametric TV-FRF estimation procedure using arbitrary excitations in the presence of missing data [15].

The nonparametric approaches via concatenation of records [16] to remove the missing data gaps, or the overlapping of windows [17] could be used to solve the missing data problem for TV-FRF measurements. However, in both cases the number of gaps must be much smaller than the total number of samples, which makes these techniques feasible for a few bursts of missing samples only.

The paper is organised as follows. Section II defines the class of time-varying nonlinear systems and the class of excitation signals for which the theory applies, and recalls that the estimation of the TV-FRF can be reformulated as an FRF estimation problem. Since FRF estimation in the presence of missing data is the core of the proposed algorithm, it is briefly described in Section III. Section IV reveals the peculiarities of the impact of periodically and non-periodically missing samples on the discrete Fourier transform (DFT). Based on these results, the proposed nonparametric estimation algorithm is developed in Section V. Next, the robustness of the proposed method w.r.t. the considered class of nonlinear time-varying systems is illustrated on simulations (Section VI) and real measurements (Section VII). Finally, some conclusions are drawn in Section VIII.

II. Time-Varying Dynamics – A Short Introduction

This section provides some essential background information necessary for understanding the remainder of the paper.

A. Linear Time-Varying Systems

Define $g(t,\tau)$ as the response of a linear time-varying system to a Dirac impulse $\delta(t-\tau)$ at time instant τ. $g(t,\tau)$ is called the time-varying impulse response, where t is the response time, and τ the impulse time. Taking the Fourier transform w.r.t. τ of the time-varying kernel $k(t,\tau) = g(t, t-\tau)$ gives the time-varying frequency response function (TV-FRF) $G(j\omega, t)$ [18], [19]

$$G(j\omega,t) = \int_{-\infty}^{+\infty} k(t,\tau)e^{-j\omega\tau}d\tau \tag{1}$$

where the lower integration limit is replaced by 0 for causal systems ($g(t,\tau) = 0$ for $t < \tau \Rightarrow k(t,\tau) = 0$ for $\tau < 0$). Other definitions exist [20], but $G(j\omega, t)$ is the only TV-FRF that has the following two properties

1) The steady state response to $\sin(\omega_0 t)$ equals $|G(j\omega_0,t)|\sin(\omega_0 t + \angle G(j\omega_0,t))$
2) The transient response $y_0(t)$ to an input $u_0(t)$ is given by $y_0(t) = L^{-1}\{G(s,t)U_0(s)\}$ where $L^{-1}\{\}$ is the inverse Laplace transform and $U_0(s) = L\{u_0(t)\}$, with $L\{\}$ the Laplace transform.

Both are natural extensions of the properties of the FRF of an LTI system.

If $G(s,t)$ is a smooth function of time for $t \in [0,T]$, then it can be expanded in series as

$$G(s,t) = \sum_{p=0}^{\infty} G_p(s)f_p(t) \text{ for } t \in [0,T] \tag{2}$$

where $f_p(t)$, $p = 0,1,\ldots$, are a complete set of basis functions, and where $G_p(s)$ are the complex coefficients of the series expansion that can be interpreted as transfer functions of LTI systems. Without any loss in generality we can impose the following constraints on the basis functions:

$$f_0(t) = 1 \text{ and } \frac{1}{T}\int_0^T f_p(t)dt = 0 \text{ for } p > 0 \tag{3}$$

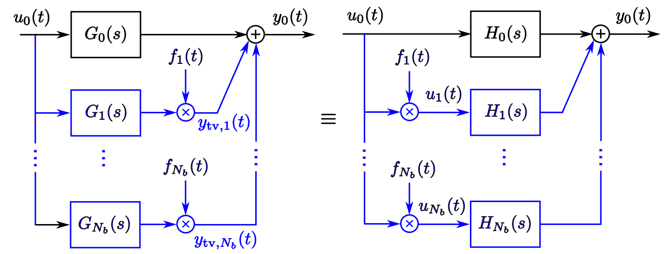

Figure 1. Direct (left) and indirect (right) models of the class of linear time-varying systems considered: time-invariant (black) and time-varying (blue) dynamics. The dynamics are related to each other by (5).

Since estimating nonparametrically an infinite number of FRFs is not feasible, the class of linear time-varying systems considered in this paper is limited to those systems for which the infinite sum (2) can be truncated.

Assumption 1 (class of linear time-varying systems considered): The time-varying transfer function can be written as

$$G(s,t) = \sum_{p=0}^{N_b} G_p(s)f_p(t) \text{ for } t \in [0,T] \tag{4}$$

where $f_p(t) = l_p(2t/T-1)$ with $l_p(x)$, $x \in [-1,1]$, Legendre polynomials of degree p [21], and where $G_p(s)$ are smooth functions of s.

Note that the basis functions in (4) satisfy the constraints (3). Eq. (4) is called the direct model in the sequel of this paper. Combining (4) with $y_0(t) = L^{-1}\{G(s,t)U_0(s)\}$ gives the left block diagram in Fig. 1, where each branch corresponds to a term in the sum (4). Using (3), it can be seen that the first term $G_0(s)$ in the sum (4) equals the mean value of $G(s,t)$ over $[0,T]$. Within the class of stationary excitations, $G_0(s)$ is also the best (in least squares sense) linear time-invariant (BLTI) approximation of $G(s,t)$ [22].

It is possible to estimate nonparametrically the dynamics $G_p(j\omega)$ from the skirts in the repose spectrum of the time-varying system to a periodic excitation [23]. However, the "skirts" approach needs sufficient spacing between the excited harmonics and, therefore, has the drawback of a limited frequency resolution of the TV-FRF measurement. As explained in the sequel, this issue can be circumvented by transforming the direct model into an equivalent representation.

First, the output gains in the left block diagram of Fig. 1 are shifted to the input. This results in the right block diagram of Fig. 1, which is called the indirect model in the sequel of this paper. The dynamics of the indirect and direct models are related by (see [24])

$$
\begin{aligned}
G_p(s) = H_p(s) + \frac{2}{T}(2p+1) \sum_{i=0}^{\left\lfloor \frac{N_b-p-1}{2} \right\rfloor} H^{(1)}_{2i+1+p}(s) + \\
\frac{4}{T^2} \sum_{i=1}^{\left\lfloor \frac{N_b-p}{2} \right\rfloor} \beta_{2i,p} H^{(2)}_{2i+p}(s) + O\left(T^{-3}\right)
\end{aligned} \tag{5}
$$

with $H_p^{(n)}(s)$ the nth order derivative of $H_p(s)$ w.r.t. s, $\lfloor x \rfloor$ the largest integer smaller than or equal to x, and $\beta_{2i,p}$ coefficients defined as

$$
\begin{aligned}
\beta_{2i,p} &= \gamma_p + \delta_p (i-1) + \mu_p (i-1)^2 \\
\gamma_p &= 1.5 + 4p + 2p^2 \\
\delta_p &= 2.5 + 6p + 2p^2 \\
\mu_p &= 1 + 2p
\end{aligned} \tag{6}
$$

The $O(T^{-3})$ bias error in (5) depends on higher order (> 2) derivatives of $H_p(s)$ w.r.t. s. However, since the derivatives in (5) are calculated numerically along the $j\omega$-axis via central differences with an $O(T^{-3})$ approximation error, it makes no sense to include these higher order (> 2) derivatives in the formula.

Next, it can be verified that the inputs $u_p(t) = u_0(t) f_p(t)$ of the $H_p(s)$ blocks in Fig. 1 are linearly independent over $[0, T]$, because the functions $f_p(t)$, $p = 0, 1, \ldots, N_b$, form a basis (see [24], Lemma 4). As a consequence, the indirect model can be interpreted as an $N_b + 1$ input, single output LTI system, whose dynamics can be estimated using standard nonparametric estimation techniques for multivariate systems. Proceeding in this way no restrictions are imposed on the spacing between excited frequencies and, hence, on the frequency resolution.

Note that the response of the indirect model can be calculated as $Y_0(s) = L\{H(s,t) u_0(t)\}$ with

$$
H(s,t) = \sum_{p=0}^{N_b} H_p(s) f_p(t) \tag{7}
$$

which is a generalisation of the LTI formula $Y_0(s) = L\{H(s) u_0(t)\}$. Eq. (7) is an alternative definition of the time-varying transfer function that does not satisfy properties 1) and 2) of the TV-FRF (1) introduced by Zadeh [18], [19].

B. Nonlinear Time-Varying Systems

The following assumption defines a specific class of nonlinear time-varying systems, for which the estimation algorithm presented in Section V is applicable.

Assumption 2 (class of nonlinear time-varying systems considered): The response of the nonlinear time-varying system can be split into a nonlinear time-invariant part and a linear time-varying part satisfying Assumption 1. In addition, the steady state response of the nonlinear time-invariant part to a periodic input is periodic with the same period as the input.

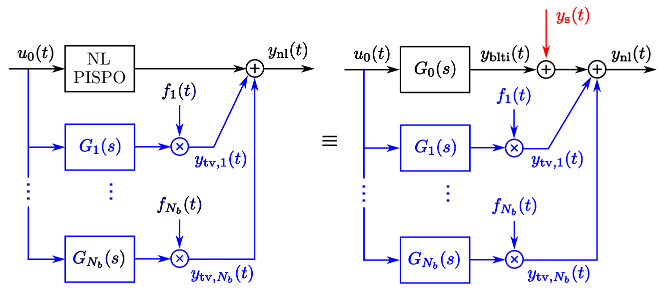

Figure 2. Direct model of the class of nonlinear time-varying systems considered. $G_0(s)$ (black) is the best linear time invariant (blti) approximation of the nonlinear period-in-same-period-out (PISPO) time-varying system, and $y_{\rm s}(t)$ (red) is the stochastic nonlinear distortion which is uncorrelated with – but not independent of – the input $u_0(t)$. The linear time-varying part is depicted in blue.

Sub-harmonics and chaotic behaviour are excluded by this assumption, but hard nonlinearities such as, for example, saturation or dead zones, are allowed. Fig. 2 shows a block diagram of the corresponding class of nonlinear period-in-same-period-out (PISPO) time-varying systems. Note that Assumption 2 is reasonable for weakly time-varying systems.

The (TV-)FRF measurements are performed using the following class of periodic excitation signals.

Assumption 3 (class of excitation signals considered): The excitation $u_0(t)$ is a random phase multisine

$$
u_0(t) = \sum_{h=H_1}^{H_2} A_h \sin(h\omega_0 t + \phi_h) \tag{8}
$$

with ϕ_h independent (over h) randomly chosen phases s.t. $\mathbb{E}\{e^{j\phi_h}\} = 0$, A_h user defined amplitudes, and $0 \leq H_1 < H_2$ with $H_1, H_2 \in \mathbb{N}$.

Under Assumptions 2 and 3 the nonlinear time-invariant block in Fig. 2 can be replaced by its best (in least squares sense) linear approximation $G_0(s)$ and an output residual $y_{\rm s}(t)$ that is uncorrelated with – but not independent of – the excitation $u_0(t)$ [25], [26]. The resulting right block diagram in Fig. 2 can be redrawn in two different ways (see Fig. 3), where $G(s,t)$ (top right) and $G_0(s)$ (bottom right) represent, respectively, the best (in least squares sense) linear time-varying (BLTV) and time-invariant (BLTI) approximations of the considered class of nonlinear time-varying systems. The term "best" in BTLV and BLTI is motivated by the following properties of the output residuals $y_{\rm s}(t)$ and $y_{\rm tv}(t) = \sum_{p=1}^{N_b} y_{{\rm tv},p}(t)$, where $y_{{\rm tv},p}(t) = L^{-1}\{G_p(s) U_0(s)\} f_p(t)$ (see Fig. 2).

Property 1 (output residuals BLTV and BLTI approximations): Denote $Y_{\rm S}(k)$ and $Y_{\rm TV}(k)$ as the discrete Fourier transforms (DFTs) $Y_{\rm S}(k) = {\rm DFT}(y_{\rm s}(nT_{\rm s}))$ and $Y_{\rm TV}(k) = {\rm DFT}(y_{\rm tv}(nT_{\rm s}))$, with $T_{\rm s}$ the sampling period and

$$
X(k) = {\rm DFT}(x(nT_{\rm s})) = \frac{1}{\sqrt{N}} \sum_{n=0}^{N-1} x(nT_{\rm s}) e^{-j2\pi \frac{kn}{N}}, \tag{9}
$$

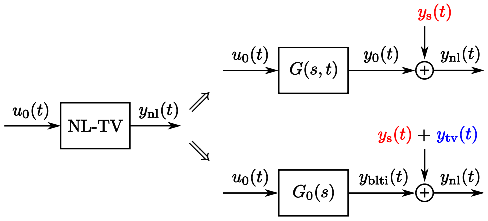

Figure 3. Best linear time-varying (bltv) $G(s,t)$ (top) and best linear time-invariant (blti) $G_0(s)$ (bottom) approximations of the considered class of nonlinear time-varying (NL-TV) systems. $y_0(t) = y_{\text{blti}}(t) + y_{\text{tv}}(t)$ with $y_{\text{blti}}(t)$ (black) and $y_{\text{tv}}(t) = \sum_{p=1}^{N_b} y_{\text{tv},p}(t)$ (blue) the response of the linear time-invariant and linear time-varying parts, respectively (see Fig. 2). $y_s(t)$ (red) represents the stochastic nonlinear distortion.

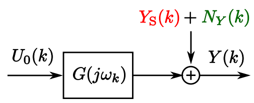

Figure 4. Measurement of the frequency response function in the presence of noise $N_Y(k)$ (green) and nonlinear distortion $Y_S(k)$ (red).

of, respectively, $y_s(t)$ and $y_{\text{tv}}(t)$. $Y_S(k)$ and $Y_{TV}(k)$ are mutually uncorrelated and uncorrelated with – but not independent of – $U_0(k)$ (proof: see [22], [26]).

III. FRF Measurement in the Presence of Missing Output Data

From Section II it follows that the nonparametric estimation of the BLTV and BLTI approximations can be simplified to the estimation of the FRF of a multiple-input, single-output LTI system (see Fig. 1, indirect model). Therefore, the basic equations of the missing data problem are briefly explained for the LTI case with known input and noisy output observations. To simplify the notations we handle here the SISO case.

Assumption 4 (stochastic framework): Known input, noisy output measurements are available. The disturbing output noise is filtered band-limited white noise [27] with DFT (9)

$$N_Y(k) = H_Y(j\omega_k)E(k) + T_{H_Y}(j\omega_k) \tag{10}$$

where $V_Y(k) = H_Y(j\omega_k)E(k)$ is the part that is uncorrelated over the frequency ($\mathbb{E}\{E(k)\overline{E(l)}\} = 0$ for $k \neq l$ and with $\overline{x}$ the complex conjugate of x) and $T_{H_Y}(j\omega_k)$ the noise transient term that is a smooth function of the frequency.

Assume that M_y consecutive samples are missing starting from time instant $K_y T_s$. Under Assumption 4 the DFT $Y^{\text{m}}(k)$ of the noisy output samples $y(nT_s)$, where the missing data is set to zero, is related to the DFT $U_0(k)$ of the known input samples $u_0(nT_s)$ as [28]

$$\begin{aligned} Y^{\text{m}}(k) = {} & G(j\omega_k)U_0(k) + T(j\omega_k) \\ & - \frac{1}{\sqrt{N}} z_k^{-K_y} I_y(z_k^{-1}, \psi) + V_Y(k) \end{aligned} \tag{11}$$

where $T(j\omega_k)$ is the sum of the noise $T_{H_Y}(j\omega_k)$ and system $T_G(j\omega_k)$ transient terms, with $z_k = \exp(j2\pi k/N)$ and $I_y(z^{-1}, \psi) = \sum_{n=0}^{M_y-1} y((K_y+n)T_s)z^{-n}$ a polynomial in z^{-1} containing the missing data ψ

$$\psi = \left[\begin{array}{ccc} y(K_y T_s) & \ldots & y((K_y + M_y - 1)T_s) \end{array}\right]^T \tag{12}$$

Note that (11) valid for one block of missing samples can easily be extended to the case of N_m blocks of missing samples.

Since the FRF $G(j\omega)$ and the transient term $T(j\omega)$ are smooth functions of $j\omega$, they can be approximated arbitrarily well in a local frequency band by a polynomial of sufficiently high degree [26]. Expanding $G(j\omega_{k+m})$ and $T(j\omega_{k+m})$ in Taylor series of degree R around, respectively, $G(j\omega_k)$ and $T(j\omega_k)$, gives

$$G(j\omega_{k+m}) = G(j\omega_k) + \sum_{r=1}^{R} g_r m^r + O((m/N)^{R+1}) \tag{13}$$

$$T(j\omega_{k+m}) = T(j\omega_k) + \sum_{r=1}^{R} t_r m^r + \frac{O((m/N)^{R+1})}{\sqrt{N}} \tag{14}$$

where the additional factor $1/\sqrt{N}$ in (14) originates from the fact that the transient term $T(j\omega)$ is an $O(N^{-1/2})$. The unknown complex parameters in (13) and (14) are collected in the vector θ_k

$$\theta_k = \left[\begin{array}{cccccccc} G(j\omega_k) & g_1 & \ldots & g_R & T(j\omega_k) & t_1 & \ldots & t_R \end{array}\right]^T \tag{15}$$

Combining (11)–(15) results in

$$\begin{aligned} Y^{\text{m}}(k+m) &= K_k(m)\theta_k + W_{k+m}\psi + V_Y(k+m) \\ K_k(m) &= \left[\begin{array}{cc} p_R(m)U_0(k+m) & p_R(m) \end{array}\right] \\ p_R(m) &= \left[\begin{array}{cccc} 1 & m & \ldots & m^R \end{array}\right] \\ W_{k+m} &= -\frac{1}{\sqrt{N}} z_{k+m}^{-K_y} \left[\begin{array}{cccc} 1 & z_{k+m}^{-1} & \ldots & z_{k+m}^{-(M_y-1)} \end{array}\right] \end{aligned} \tag{16}$$

Expressing (16) in a local frequency band $m = -n, -n+1, \ldots, n$ at all frequencies of interest $k = 1, 2, \ldots, F$ gives a sparse $(2n+1)F \times (2(R+1)F + M_y)$ set of linear complex equations in the local complex parameters $\theta_1, \theta_2, \ldots, \theta_F$ (15) and the global real parameters ψ (12). Choosing $2n + 1 > 2(R+1) + M_y/(2F)$, the sparse overdetermined set of linear equations is solved time- and memory-efficiently in least squares sense using QR-decompositions, and from the residuals of the least squares solution an estimate of the noise variance $\text{var}(V_Y(k))$, $k = 1, 2, \ldots, F$, is obtained (see [28] for the details).

IV. Influence Missing Data on the DFT Spectrum

Fig. 5 shows P periods of the noiseless response $y_0(t)$ of a time-varying system to a random phase multisine $u_0(t)$ (8). The DFT of the sampled response $y_0(nT_s)$, $n = 0, 1, \ldots, NP-1$, where each period contains N samples,

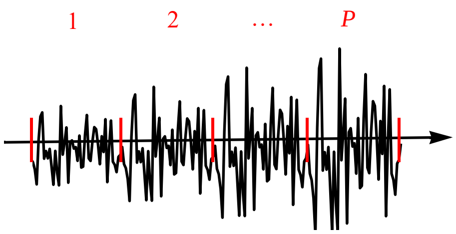

Figure 5. P periods of the response of a time-varying system to a random phase multisine (8).

$$Y_0(k) = \frac{1}{\sqrt{NP}} \sum_{n=0}^{NP-1} y_0(nT_s) e^{-j2\pi \frac{kn}{NP}} \tag{17}$$

can be split into two sets of frequencies:

1) The "harmonic" DFT frequencies $\mathbb{K}_p = \{k = rP, r = 0, 1, \ldots, N/2\}$, at which input signal energy of $u_0(t)$ (8) can be present.
2) The "non-harmonic" DFT frequencies $\mathbb{K}_{np} = \{k = rP + l, r = 0, 1, \ldots, N/2 - 1, l = 1, 2, \ldots, P - 1\}$, at which no input signal energy of $u_0(t)$ (8) can be present.

Lemma 1. *At the "harmonic" DFT frequencies $k \in \mathbb{K}_p$, the DFT (17) only depends on the mean value over the periods of the samples $\overline{y_0}(nT_s) = P^{-1} \sum_{p=0}^{P-1} y_0((n+pN)T_s$, $n = 0, 1, \ldots, N-1$. At the "non-harmonic" DFT frequencies $k \in \mathbb{K}_{np}$, the DFT (17) depends on the difference between the samples and their mean value over the periods $y_0((n+pN)T_s) - \overline{y_0}(nT_s)$, $n = 0, 1, \ldots, N-1$ and $p = 0, 1, \ldots, P-1$.*

Proof: We evaluate (17) at the "harmonic" DFT frequencies $k \in \mathbb{K}_p$ and split the sum into P sums over N samples

$$\begin{aligned} Y_0(rP) &= \frac{1}{\sqrt{NP}} \sum_{n=0}^{NP-1} y_0(nT_s) e^{-j2\pi \frac{rn}{N}} &(18)\\ &= \frac{1}{\sqrt{NP}} \sum_{p=0}^{P-1} \sum_{n=0}^{N-1} y_0((n+pN)T_s) e^{-j2\pi \frac{r(n+pN)}{N}} \\ &= \sqrt{\frac{P}{N}} \sum_{n=0}^{N-1} \overline{y_0}(nT_s) e^{-j2\pi \frac{rn}{N}} &(19)\end{aligned}$$

where the last equality uses $e^{-j2\pi rp} = 1$ and next interchanges the sums over p and n. Eq. (19) proves the first statement.

Following the same lines at the "non-harmonic" DFT frequencies $k \in \mathbb{K}_{np}$ we find

$$\begin{aligned} Y_0(rP+l) &= \frac{1}{\sqrt{NP}} \sum_{n=0}^{NP-1} y_0(nT_s) e^{-j2\pi \frac{(rP+l)n}{NP}} &(20)\\ &= \frac{1}{\sqrt{NP}} \sum_{p=0}^{P-1} \sum_{n=0}^{N-1} y_0((n+pN)T_s) e^{-j2\pi \frac{(rP+l)(n+pN)}{NP}} \\ &= \frac{1}{\sqrt{NP}} \sum_{n=0}^{N-1} \widetilde{Y}_0(l,n) e^{-j2\pi \frac{(rP+l)n}{NP}} &(21)\end{aligned}$$

where the last equality uses $e^{-j2\pi rp} = 1$ and with $\widetilde{Y}_0(l,n) = \sum_{p=0}^{P-1} y_0((n+pN)T_s) e^{-j2\pi lp/P}$. Replacing $y_0((n+pN)T_s)$ by $y_0((n+pN)T_s) - \overline{y_0}(nT_s)$ in $\widetilde{Y}_0(l,n)$ does not affect the sum because $\sum_{p=0}^{P-1} e^{-j2\pi lp/P} = 0$ for $l = 1, 2, \ldots, P-1$. Hence, (21) proves the second statement. ■

According to the time instants at which the samples are missing, the missing data can be split into two sets:

1) *Periodically missing data:* the data is missing at one or more set(s) of "periodic" time instants $\mathbb{T}_n = \{t = (n+pN)T_s, p = 0, 1, \ldots, P-1\}$ with $0 \leqslant n \leqslant N-1$.
2) *Non-periodically missing data:* no subset of the time instants at which data is missing belongs to any set $\mathbb{T}_n$ with $0 \leqslant n \leqslant N-1$.

The non-periodically missing output data contributes to the output DFT (17) at all DFT frequencies. Although this is also true for the periodically missing data, the situation is more complicated as stated in the following lemma.

Lemma 2. *At the "harmonic" DFT frequencies $k \in \mathbb{K}_p$, the DFT (17) depends on the non-periodically missing samples and the mean value over the periods of the periodically missing samples. At the "non-harmonic" DFT frequencies $k \in \mathbb{K}_{np}$, the DFT (17) depends on the non-periodically missing samples and on the difference between the samples and their mean value over the periods of the periodically missing samples.*

Proof: The known samples in (18) and (20) are set to zero. If the data is missing at non-periodic time instants, then the resulting sums (18) and (20) over the missing samples can never be split into P sums of samples missing over one period. Hence, (18) and (20) cannot be written under the form (19) and (21), respectively, which proves the statements about the non-periodically missing samples. If the data is missing at one or more set(s) $\mathbb{T}_n$ of "periodic" time instants, then the resulting sums (18) and (20) over the missing samples can be written under the form (19) and (21), respectively, which proves the statements about the periodically missing samples. ■

Remark 3. Samples missing at the borders of the record ($K_y = 0$ or $K_y = N - M_y$ in (11)) are not identifiable because both the transient term $T(j\omega)$ and the missing data contribution $z^{-K_y} T_y(z^{-1}, \psi)$ in (11) can be approximated very well by a polynomial in a local frequency band (see [28]). For periodic excitations this identifiability problem extends to samples missing at the borders of the periods [3].

V. Estimation Algorithm

In the remainder of this section we first handle the case of known input, noisy output measurements of systems operating in open loop (Section V-A). Next, these results are generalised to noisy input, noisy output measurements of systems operating in closed loop (Section V-B). Finally, Section V-C discusses the parameters that influence the mean square error of the nonparametric TV-FRF estimates.

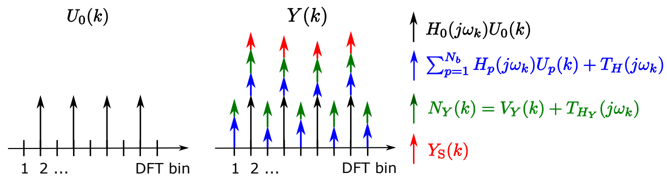

Figure 6. DFT $Y(k)$ of two consecutive periods of the measured steady state response of the best linear time-varying approximation $G(s,t)$ (see, Fig. 3, top right block diagram) of the considered class of nonlinear time-varying systems to a random phase multisine $U_0(k)$. The time-varying transfer function $G(s,t)$ is replaced by its indirect model (see Fig. 1, right block diagram). Black arrows in $Y(k)$: response time-invariant part indirect model; blue arrows: response time-varying part indirect model; green arrows: output noise; and red arrows: nonlinear distortion.

A. Known Input, Noisy Output Measurements of Systems Operating in Open Loop

Under Assumptions 1–4 the DFT (17) of two consecutive periods of the measured steady state response $y(t)$ of the class of NL-TV systems considered (Assumption 2) excited by a random phase multisine excitation $u_0(t)$ (8) is given by Fig. 6. To construct this figure, the best linear time-varying approximation $G(s,t)$ of the NL-TV system (Fig. 3, top right block diagram) has been replaced by its indirect model (Fig. 1, right block diagram). From Fig. 6 it can be seen that the output $Y(k)$ does not depend on the LTI branch (black arrows) and the nonlinear distortions (red arrows) at the non-periodic DFT frequencies (DFT bins 1, 3, 5, $\ldots$). This observation together with Lemma 2 forms the basis of the 3-step estimation procedure explained in the sequel of this section. The procedure is elaborated for a time-varying system with n_u inputs $u_0(t)$ and n_y outputs $y(t)$. In the multivariate case $u_0(t)$ is a vector of random phase multisines with independently chosen phases.

STEP 1 – Modeling of the time-varying branches in the indirect model (see Fig. 7).

1) Choose the initial number of time-varying branches N_b, the initial degree R of the local polynomial method (LPM), and the degrees of freedom of the residuals of the LPM estimate which are quantified by [3], [29]

$$\mathrm{dof_n} = 2n\left(1 - \frac{M_y^{\max}}{2F_{\mathrm{np}}}\right) - (R+1)(n_u N_b + 1) \qquad (22)$$

with $M_y^{\max}$ the maximum (over the n_y outputs) number of missing output samples, and $F_{\mathrm{np}} = N(P-1)/2 - 1$ the total number of non-periodic DFT frequencies. $n_u N_b$ is the number of known inputs $u_p(t)$, $p = 1, 2, \ldots, N_b$, of the time-varying branches in the indirect model (see Fig. 1), and $2n$ is the local number of non-periodic DFT frequencies centered around $k = rP$ which are used for the local polynomial approximation of degree R ((13) and (14) with $m = -n, -n+1, \ldots, -1, 1, \ldots, n$). Choosing $\mathrm{dof_n}$ and R fixes the local bandwidth $2n$ via (22).

2) Calculate the DFT spectra (17) of the auxiliary inputs $u_p(t) = u_0(t)f_p(t)$, $p = 0, 1, \ldots, N_b$, in the indirect

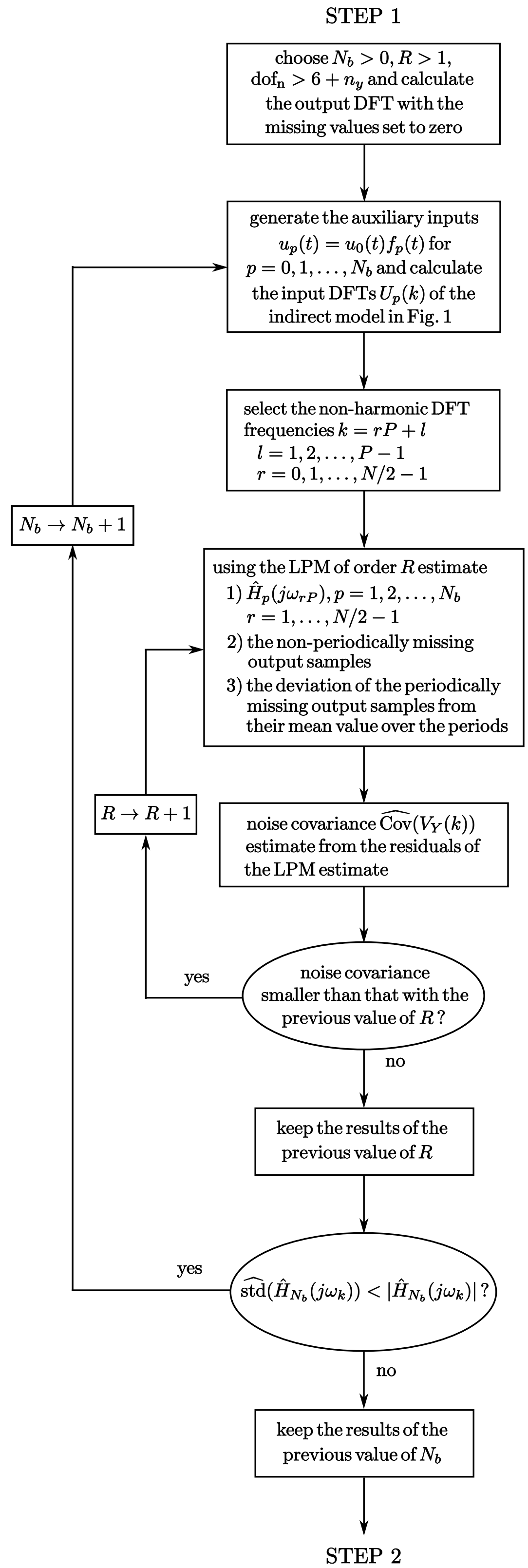

Figure 7. First step of the estimation algorithm for an n_u input, n_y output system: estimation of the N_b time-varying branches in the indirect model of Fig. 1, the non-periodically missing samples, and the deviation of the periodically missing samples from their mean value over the P periods. R is the order of the local polynomial method (LPM), which is a linear least squares procedure [26], [28]. The degrees of freedom of the residuals of the LPM estimate are quantified by $\mathrm{dof_n}$ (22). P and N are, respectively, the number of observed excitation periods and the number of samples per period.

model in Fig. 1, and select the non-periodic DFT frequencies $k = rP + l$, $r = 0, 1, \ldots, N/2 - 1$ and $l = 1, 2, \ldots, P - 1$.

3) Using the local polynomial approximation of degree R at the non-periodic DFT frequencies ((13) and (14) with $m = -n, -n+1, \ldots, -1, 1, \ldots, n$), estimate via (16) (i) the FRFs of the time-varying branches in the indirect model at the periodic DFT frequencies ($\hat{H}_p(j\omega_{rP})$, $p = 1, 2, \ldots, N_b$), (ii) the non-periodically missing output samples, and (iii) the deviation of the periodically missing output samples from their mean value over the periods. In this step the constraint $\sum_{p=0}^{P-1} \hat{y}((n + pN)T_s) = 0$ is imposed for each set $\mathbb{T}_n$ of periodically missing samples.

4) Estimate the noise covariance $\widehat{\mathrm{Cov}}(V_Y(k))$ from the residuals of the LPM estimates [29]. Increase the degree of the local polynomial approximation R if the noise covariance is smaller than that obtained for the previous lower value of R. Increase the number of time-varying branches N_b if the estimated noise standard deviation of $\hat{H}_{N_b}(j\omega_k)$ is smaller than $\left|\hat{H}_{N_b}(j\omega_k)\right|$ (calculated element-wise). This iterative procedure reduces the bias error on the TV-FRF estimate at the noise level.

STEP 2 – Modeling of the time-invariant branch in the indirect model (see Fig. 8, left column).

1) Fill out the estimated non-periodically missing output samples in the output DFT giving $\hat{Y}^{\mathrm{m}}(k)$ (the periodically missing samples are still set to zero), and choose the degrees of freedom of the residuals of the LPM estimate which are quantified by [3], [29]

$$\mathrm{dof}_{\mathrm{NL}} = (2n_{\mathrm{NL}} + 1)(1 - \frac{M_{y,\mathrm{per}}^{\max}}{2F_{\mathrm{p}}}) - (R+1)n_u \quad (23)$$

with $M_{y,\mathrm{per}}^{\max}$ the maximum (over the n_y outputs) number of periodically missing output samples, and $F_{\mathrm{p}} = N/2 - 1$ the number of periodic DFT frequencies (DC and Nyquist are excluded). n_u is the number of known inputs $u_0(t)$ of the time-invariant branch in the indirect model, and $2n_{\mathrm{NL}} + 1$ is the local number of periodic DFT frequencies centered around $k = rP$ used for the local polynomial approximation of degree R ((13) with $m = -n_{\mathrm{NL}}, -n_{\mathrm{NL}}+1, \ldots, -1, 0, 1, \ldots, n_{\mathrm{NL}}$). Choosing $\mathrm{dof}_{\mathrm{NL}}$ and R fixes the local bandwidth $2n_{\mathrm{NL}}+1$ via (23).

2) Select the periodic DFT frequencies $k = rP$, $r = 1, 2, \ldots, N/2 - 1$, and subtract the contribution of the time-varying branches and the transient term obtained in step 1.3 from the output DFT $\hat{Y}^{\mathrm{m}}(k)$

$$\hat{Y}^{\mathrm{m}}(k) - \sum_{p=1}^{N_b} \hat{H}_p(j\omega_k)U_p(k) - \hat{T}_{\mathrm{ind}}(j\omega_k) \quad (24)$$

where $T_{\mathrm{ind}}(j\omega_k) = T_{H_Y}(j\omega_k) + T_H(j\omega_k)$ with $T_{H_Y}(j\omega_k)$ and $T_H(j\omega_k)$, respectively, the noise and system transient terms (see Fig. 6).

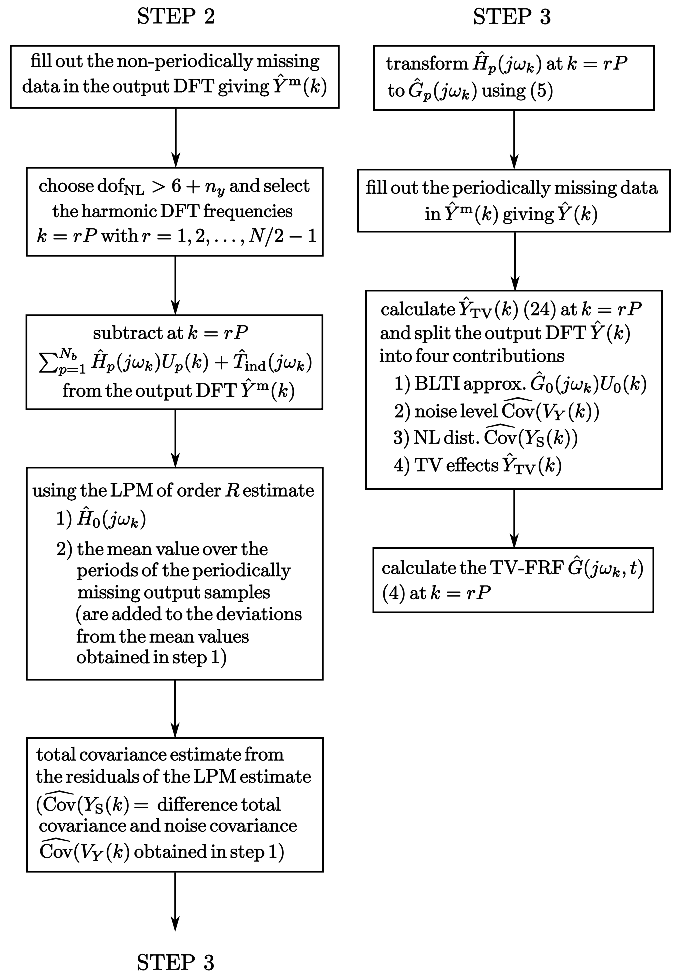

Figure 8. Second (left column) and third (right column) steps of the estimation algorithm. Step 2: estimation of the time-invariant branch in the indirect model of Fig. 1, and the mean value over the P periods of the periodically missing samples. $T_{ind}(j\omega_k)$ is the sum of the noise $T_{H_Y}(j\omega_k)$ and the system $T_H(j\omega_k)$ transient terms in Fig. 5. The degrees of freedom of the residuals of the LPM estimate of degree R are quantified by $\mathrm{dof}_{\mathrm{NL}}$ (23). Step 3: transformation of the indirect to the direct model, and calculation of the best linear time-invariant (BLTI) approximation and the time-varying frequency response function (TV-FRF).

3) Using the local polynomial approximation of degree R at the periodic DFT frequencies ((13) with $m = -n_{\mathrm{NL}}, -n_{\mathrm{NL}} + 1, \ldots, -1, 0, 1, \ldots, n_{\mathrm{NL}}$), estimate via (16) (i) the FRF of the time-invariant branch in the indirect model $\hat{H}_0(j\omega_k)$, and (ii) the mean value over the periods of the periodically missing output samples. Add the mean value of the periodically missing samples to the deviations from the mean value obtained in step 1.

4) Calculate the total covariance (= sum noise covariance and covariance nonlinear distortions) from the residuals of the LPM estimates in step 2.3 [3]. Subtracting the noise covariance estimate $\widehat{\mathrm{Cov}}(V_Y(k))$ obtained in step 1 from the total covariance gives an estimate of the covariance of the nonlinear distortions $\widehat{\mathrm{Cov}}(Y_{\mathrm{S}}(k))$.

STEP 3 – Transformation of the indirect to the direct model (see Fig. 8, right column)

1) Transform the indirect model $\hat{H}_p(j\omega_k)$ at the periodic DFT frequencies $k = rP$ to the direct model $\hat{G}_p(j\omega_k)$ using (5), where the derivatives are replaced by central differences [24]. The time-invariant branch $\hat{G}_0(j\omega_k)$ of the direct model is the best linear time-invariant approximation of the nonlinear time-varying system (see Figs. 2 and 3).
2) Fill out the estimated periodically missing samples in the output DFT $\hat{Y}^{\mathrm{m}}(k)$ giving $\hat{Y}(k)$, and calculate the output contribution of the time-varying branches in the direct model at the periodic DFT frequencies $k = rP$ as

$$\hat{Y}_{\mathrm{TV}}(k) = \mathrm{DFT}(\sum_{p=1}^{N_b} \mathrm{IDFT}(\hat{G}_p(j\omega_k)U_0(k))f_p(t)) \quad (25)$$

where $\mathrm{IDFT}(X(k)) = \frac{1}{\sqrt{NP}}\sum_{k=0}^{NP-1} X(k)e^{j2\pi\frac{kn}{NP}}$. Using the noise covariance obtained in step 1, the covariance of the nonlinear distortions obtained in step 2, and $\hat{Y}_{\mathrm{TV}}(k)$ (25), the output DFT $\hat{Y}(k)$ can be split into four contributions (i) the best linear time-invariant approximation $\hat{G}_0(j\omega_k)U_0(k)$, (ii) the time-varying effects $\hat{Y}_{\mathrm{TV}}(k)$, (iii) the level of the nonlinear distortions $\widehat{\mathrm{Cov}}(Y_{\mathrm{S}}(k))$, and (iv) the noise level $\widehat{\mathrm{Cov}}(V_Y(k))$.
3) Using (4), $\widehat{\mathrm{Cov}}(V_Y(k))$ and $\widehat{\mathrm{Cov}}(Y_{\mathrm{S}}(k))$, calculate the TV-FRF $\hat{G}(j\omega_k, t)$ and its covariances due to noise and nonlinear distortions at the periodic DFT frequencies $k = rP$.

B. Noisy Input, Noisy Output Measurements of Systems Operating in Closed Loop

Note that the algorithm of Section V-A cannot be applied to noisy input, noisy output measurements where both measurements are subject to missing data. Moreover, even if no input samples are missing, due to the input noise the proposed estimation algorithm results in biased TV-FRF estimates. This is also true for noisy input-output measurements of time-varying systems operating in closed loop. To handle all these issues, a known reference signal should be available, typically the signal stored into the arbitrary waveform generator. Following the same lines of [30], the time-varying system operating in closed loop is modelled from the known reference to the noisy input-output measurements. This is a known input, noisy output problem for which the algorithm of Section V-A applies. The TV-FRF from input to output is recovered from the TV-FRFs from reference to output and from reference to input via the deconvolution algorithm developed in [30].

C. Stochastic Properties of the Estimator

Assume that the direct model (4) remains valid for $N \to \infty$ ($T = NP$). Since

1) the algorithm described in Section V-A is a linear least squares estimator with a – by construction – noise-free regression matrix (see (16)), and
2) the local polynomial approximations (13) and (14), and the transformation of the indirect to the direct model are asymptotically (for $N \to \infty$) unbiased,

it then follows that the linear least squares estimates of the TV-FRF and the missing data are asymptotically (for $N \to \infty$) unbiased. However, the TV-FRF and missing data estimates are inconsistent because adding data does not provide information about the past missing samples.

Bias Error. The bias error of the estimates has four contributions ($T = NP$):

1) the $O(N^{-(R+1)})$ bias of the local polynomial approximation of degree R of the estimated FRFs $\hat{H}_p(j\omega_k)$ in the indirect model,
2) the $O(N^{-3})$ bias due to neglecting the higher order ($>$ 2) derivatives in the transformation (5) of the indirect to the direct model [24],
3) the $O(N^{-3})$ bias due to the approximation of the first and second order derivatives in (5) by central differences [31], and
4) the bias due to a too small value of the number N_b of time-varying branches.

Note that the local bias errors due to a too small value of R (bias contribution 1) and N_b (bias contribution 4) depend on the random phase realisation of the multisine $u_0(t)$ (8). Therefore, they can be handled as being random over the frequency and they are correctly quantified by the estimated noise and total covariances in, respectively, steps 1 and 2 of the estimation algorithm.

Variance – Mean Squared Error. The noise and total covariances in steps 1 and 2 of the estimation algorithm are estimated via the magnitude squared residuals of the local polynomial approximations. If the bias contributions 1 and/or 4 are above the noise level, then the magnitude squared residuals are an estimate of the mean squared error (sum of the variance and the bias squared). At the end of step 2 we have an estimate of the FRFs $H_p(j\omega_k)$ together with their noise ($p = 0, 1, \ldots, N_b$) and total ($p = 0$) covariances. Using (5), the noise ($p = 0, 1, \ldots, N_b$) and total ($p = 0$) covariances of the FRFs $G_p(j\omega_k)$ are obtained. These results are then used to calculate the noise and total covariances of the TV-FRF (1).

Missing Data Pattern. Identifiability of the missing data requires that no missing samples are allowed at the borders of the excitation periods. Besides this condition, any missing data pattern can be handled by the method described in Section V-A, for example, randomly missing data, bursts of missing data, and clipping. However, some patterns are more noise sensitive than others. Indeed, from extensive simulations it follows that clipping results in a higher sensitivity to the disturbing noise than a randomly missing pattern [32]. The rationale for this is that the systematic removal of the extreme signal values decreases the signal-to-noise ratio (SNR) of the observed samples, while the SNR of the observed samples remains the same for random (independent of the signal) missing data patterns.

VI. Simulation Example: Time-Varying State Space Model

To illustrate the robustness of the proposed method w.r.t. the considered class of time-varying systems (Assumption 1), we take as simulation example a time-varying state space model for which the finite sum (4) is an approximation.

A. Simulation Setup

The time-varying state space model

$$\begin{aligned} \frac{dx(t)}{dt} &= A(t)x(t) + B(t)u_0(t) \\ y_0(t) &= C(t)x(t) \end{aligned} \tag{26}$$

mimics a vibrating mechanical structure with time-varying (anti-)resonance frequencies f_i and damping ratios ζ_i. The state space matrices $A(t)$, $B(t)$, and $C(t)$ vary linearly in time

$$\begin{aligned} A(t) &= A_1 + (A_2 - A_1)t/T \\ B(t) &= B_1 + (B_2 - B_1)t/T \quad \text{for } t \in [0, T] \\ C(t) &= C_1 + (C_2 - C_1)t/T \end{aligned} \tag{27}$$

where (A_r, B_r, C_r), $r = 1, 2$, in (27) are the controller canonical forms of a fourth order transfer function

$$\frac{\frac{s^2}{\omega_3^2} + 2\zeta_3\frac{s}{\omega_3} + 1}{\left(\frac{s^2}{\omega_1^2} + 2\zeta_1\frac{s}{\omega_1} + 1\right)\left(\frac{s^2}{\omega_2^2} + 2\zeta_2\frac{s}{\omega_2} + 1\right)} \tag{28}$$

with $\omega_i = 2\pi f_i$, $i = 1$, 2 and 3, and where $f_1 = 10\,\text{Hz}$, $\zeta_1 = 0.7$, $f_2 = 20\,\text{Hz}$, $\zeta_2 = 0.4$, $f_3 = 13\,\text{Hz}$, $\zeta_3 = 0.1$ for $r = 1$, and $f_1 = 12\,\text{Hz}$, $\zeta_1 = 0.6$, $f_2 = 22\,\text{Hz}$, $\zeta_2 = 0.3$, $f_3 = 16\,\text{Hz}$, $\zeta_3 = 0.1$ for $r = 2$. The input $u_0(t)$ is a random phase multisine (8) with uniformly $[0, 2\pi)$ distributed phases ϕ_h, and constant amplitudes $A_h = A$ chosen such that the rms value of $u_0(t)$ equals 1. It excites the frequency band $[2\,\text{Hz}, 25\,\text{Hz}]$ ($H_1 = 40$, $H_2 = 500$, $f_0 = \omega_0/(2\pi) = f_s/N$ with $f_s = 300\,\text{Hz}$ and $N = 6000$), and $P = 2$ periods of the transient response $y_0(t)$ of (26), with $T = 2/f_0$, to $u_0(t)$ are calculated using the Matlab solver ode45 with the relative and absolute tolerances set to, respectively 10^{-10} and 10^{-15}. The rms value of $y_0(t)$ equals 0.59.

No noise is added to the simulated output $y_0(t)$ because we want to quantify the bias error of the estimates due to (i) the local polynomial approximation of degree R of the FRFs and the transient term in (13) and (14), (ii) the finite number N_b of time-varying branches in (4), and (iii) the transformation from the indirect to the direct model (5). The TV-FRF $G(j\omega_k, t)$ is estimated for the full data set (no missing samples) and two missing output data patterns: 30% clipping, and 40% randomly missing samples where half of the missing values lie on a periodic grid. To avoid the identifiability issues described in [3], no missing values are allowed at the borders of the excitation periods and for each period the missing output samples are located within $[0.03, 0.97]/f_0$.

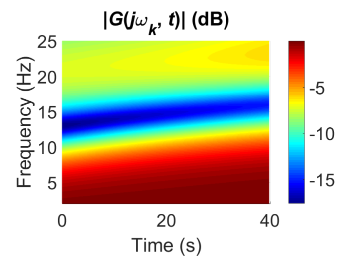

Figure 9. Time-frequency plot of the magnitude of the time-varying frequency response function – Simulation example.

B. Results

Following the procedure described in Section V-A, the values of the degree R of the local polynomial approximation and the number N_b of time-varying branches are determined from the simulated data. Using the degrees of freedom $\text{dof}_\text{n} = 20$ in step 1 and $\text{dof}_\text{NL} = 20$ in step 2 it follows that $N_b = 4$ time-varying branches in the direct model (4) and a local polynomial approximation of degree $R = 4$ are sufficient to describe accurately the time-varying dynamics for each of the three cases (no missing data, 30% clipping, and 40% randomly missing data). This results in a local number of frequencies $2n = 46, 84, 116$ in step 1 and $2n + 1 = 27, 31, 33$ in step 2 for, respectively, no missing data, 30% clipping, and 40% randomly missing data. Notice the large difference between the number of local frequencies in steps 1 and 2 for the missing data sets. This is due to the fact that all missing samples and $N_b = 4$ FRFs are estimated at the non-periodic DFT lines in step 1, while in step 2 only the mean value of the periodically missing samples and 1 FRF are estimated at the periodic DFT lines.

Figure 9 shows the estimated TV-FRF using all data (no missing samples). Since the true TV-FRF is unknown, the bias error of the full and missing data estimates is quantified by comparing the actual output DFT (no missing samples) to that predicted by the direct model (4)

$$\hat{Y}(k) = \text{DFT}\left(\sum_{p=0}^{N_b} \text{IDFT}(\hat{G}_p(j\omega_k)U_0(k))f_p(t)\right) \tag{29}$$

at the excited frequencies. The results are shown in Fig. 10. It can be seen that the bias error of the missing data estimates almost coincides with that of the full data estimate in the band $[2\,\text{Hz}, 16\,\text{Hz}]$. Above 16 Hz the bias error of the missing data estimates is larger with a maximal increase of about 20 dB around 20 Hz. The maximal relative bias error (see Fig. 10, right plot) is -77.6 dB, -70.6 dB, and -73,4 dB for, respectively, the full data, 30% clipping, and 40% randomly missing data estimates. Hence, almost 4 significant digits are correct.

Figure 11 compares the estimated to the true missing samples. It follows that the ratio of the rms value of the estimation error and the rms value of the missing samples is about 6×10^{-5} for both missing data patterns.

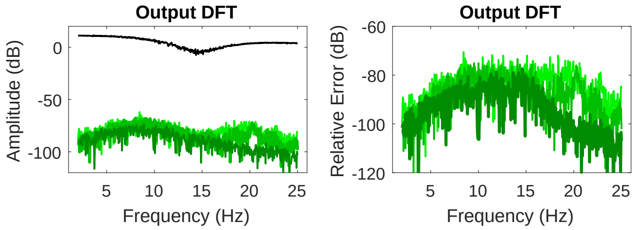

Figure 10. Comparison of the actual and the estimated output DFT spectra at the excited frequencies – Simulation example. Left: true output DFT spectrum (black line) and estimation errors of the direct model (green lines). Right: relative estimation errors. Dark green: no missing data, medium green: 40% randomly missing data, light green: 30% clipping.

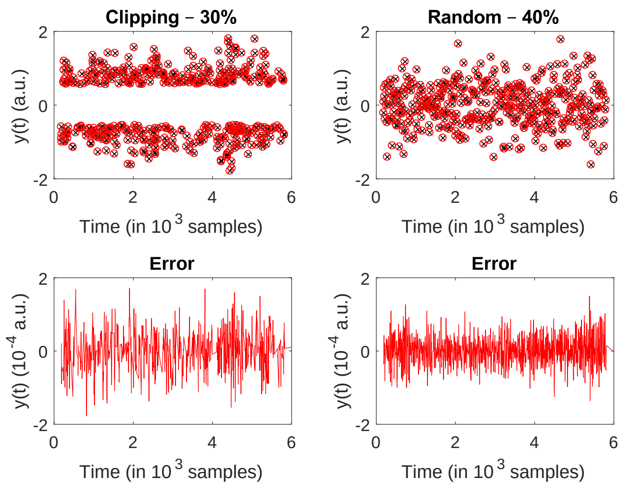

Figure 11. Comparison of the estimated and the true missing data. Top row (only one 1 out of 4 missing samples are shown): true (black x) and estimated (red o) samples – Simulation example. Bottom row (all missing samples are shown): difference between the true and estimated samples. Left column: 40% randomly missing data (0.60 rms) with an estimation error of 3.7×10^{-5} rms. Right column: 30% clipping (0.95 rms) with an estimation error of 5.6×10^{-5} rms.

C. Discussion

The results shown in Figures 10 and 11 demonstrate the robustness of the estimation algorithm w.r.t. Assumption 1. Even if the true time-varying dynamics do not satisfy exactly (4), a finite value of N_b can be found such that the bias error is smaller than the uncertainty due to the noise (and the nonlinear distortion). Clipping is more sensitive to the approximation errors (finite value N_b, local polynomial approximation of the FRFs, bias error of the indirect to direct model transformation) than the randomly missing data pattern. Indeed, for 40% clipping the maximal relative estimation error of the output DFT increases from -70.6 dB (Fig. 10, right plot) to -46 dB, which is significantly larger than the -73.4 dB of the 40% randomly missing pattern. This can be explained by the fact that clipping removes systematically the extreme signal values.

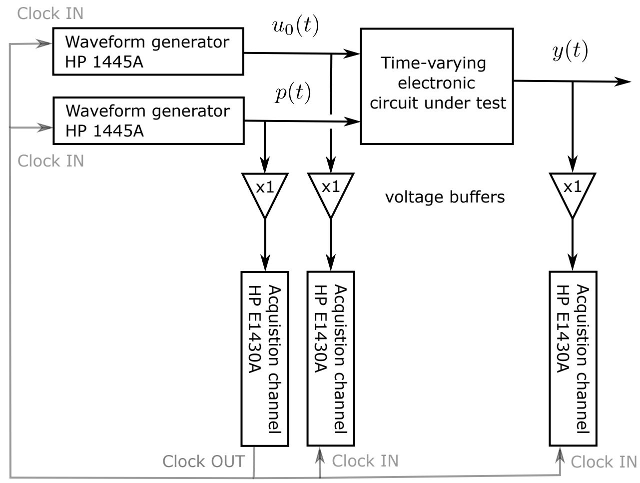

Figure 12. The measurement setup consists of 2 arbitrary waveform generators (HP 1445A), 3 voltages buffers, 3 data acquisition channels (HP E1430A), and the time-varying electronic circuit shown in Fig.13. The clock of one of the data acquisition channels serves as mother clock for the other devices (grey lines).

VII. Measurement Example: Time-Varying Electronic Circuit

The time-varying electronic circuit shown in Fig. 13 is not within the considered class of nonlinear time-varying systems (Assumption 2). Hence, this measurement example illustrates the robustness of the proposed method w.r.t. Assumption 2, and shows that the noise, the nonlinear distortion, and a relatively small time-varying effect can still be detected and quantified in the presence of a large fraction of missing samples.

Similarly to the simulation example, data is deliberately omitted in the measured response $y(t)$. By proceeding in this way it is possible (i) to choose the pattern (random or clipping) and the fraction of the missing data, and (ii) to validate the estimates of the best linear time-invariant approximation and the time-varying frequency response function based on the missing data sets, with the corresponding estimates based on all data (the true values are, after all, unknown).

A. Measurement Setup

Figure 12 shows a block diagram of the measurement setup. The input $u_0(t)$ and the gate voltage $p(t)$ of the time-varying electronic circuit shown in Fig. 13 are generated using two HP 1445A generator cards with a $50\,\Omega$ output impedance. $u_0(t)$ is a random phase multisine (8) with independent uniformly $[0, 2\pi)$ distributed phases ϕ_h, and constant amplitudes $A_h = A$ chosen such that the rms value of $u_0(t)$ equals 97 mV. It excites the frequency band $[229\,\text{Hz}, 40\,\text{kHz}]$ ($H_1 = 3$, $H_2 = 524$, $f_0 = \omega_0/(2\pi) = f_s/N$ with $f_s = 625\,\text{kHz}$ and $N = 8192$), and $P = 2$ periods of the transient response are measured. During the experiment the gate voltage $p(t)$ of the JFET transistor varies linearly between -1.612 V to -1.661 V. The rms value of the noisy response $y(t)$ equals 33 mV. To

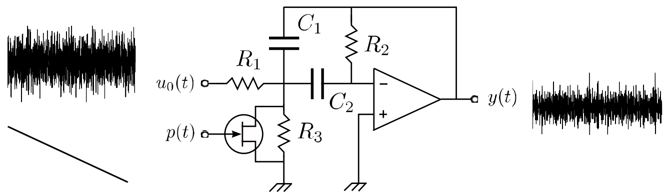

Figure 13. Transient response $y(t)$ (33 mVrms) of a second order time-varying bandpass filter to two periods of a random phase multisine $u(t)$ (97 mVrms). During the experiment the gate voltage $p(t)$ decreases linearly from -1.612 V to -1.661 V. The electronic circuit consists of a high-gain operational amplifier (CA741CE), a JFET transistor (BF245B), three resistors ($R_1 = R_2 = 10\,\text{k}\Omega$ and $R_3 = 470\,\text{k}\Omega$), and two capacitors ($C_1 = C_2 = 10\,\text{nF}$).

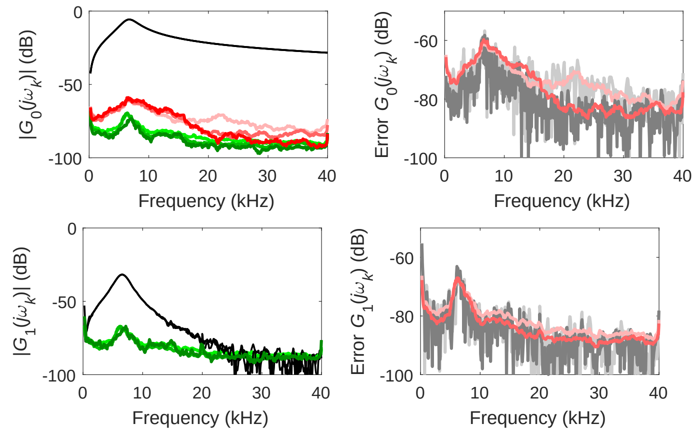

Figure 14. Estimated direct model – Measurement example. Left column: the frequency response functions (3 coinciding black lines) and their noise (green lines) and total (red lines) variances. Dark green and dark red: no missing data, medium green and medium red: 30% randomly missing data, and light green and light red: 20% clipping. Right column: Magnitude of the difference between the estimated frequency response functions using all data and the missing data sets (grey lines), and total variance of the missing data estimates (red lines). Dark grey and medium red: 30% randomly missing data, and light grey and light red: 20% clipping.

avoid loading of the time-varying electronic circuit, voltage buffers (> $5\,\text{M}\Omega$ input impedance, $50\,\Omega$ output impedance) are put in front of the three HP E1430A data acquisition channels measuring $u_0(t)$, $y(t)$, and $p(t)$ (see the triangles in Fig. 12). Coherent sampling at $f_s = 625\,\text{kHz}$ is ensured by synchronising the generator and data acquisition cards of the VXI measurement setup (grey lines in Fig. 12). Figure 13 shows the gate voltage and the measured input-output signals. Given the high signal-to-noise ratio of the input measurements (80 dB), $u_0(t)$ is considered as being known exactly.

Following the procedure described in Section V-A, the values of the degree R of the local polynomial approximation and the number N_b of time-varying branches are determined from the known input $u_0(t)$ and noisy output measurements $y(t)$ (the measured gate voltage $p(t)$ is not used in the estimation procedure). Using the degrees of freedom $\text{dof}_\text{n} = 10$ in step 1 and $\text{dof}_\text{NL} = 10$ in step 2 it follows that $N_b = 1$ time-varying branch in the direct model (4) and a local polynomial approximation of degree $R = 6$ are sufficient to describe accurately the time-varying dynamics for each of the three cases (no missing data, 20% clipping, and 30% randomly missing data). This results in a local number of frequencies $2n = 24, 34, 44$ in step 1 and $2n+1 = 17, 19, 21$ in step 2 for, respectively, no missing data, 20% clipping, and 30% randomly missing data. Similarly to the simulation, identifiability issues of samples missing at the borders of the excitation periods [3] are avoided by locating the missing data within $[0.03, 0.97]/f_0$ of each period.

B. Results

The left column of Fig. 14 shows the estimated FRFs $G_p(j\omega_k)$ of the direct model for the full data set (no missing samples) and the two missing data patterns (20% clipping and 30% randomly missing samples). It can be seen that the estimates (black lines), their noise (green lines), and the total (red lines) variances coincide, except for the total variance of the 20% clipping above 20 kHz. From the right column of Fig. 14 it follows that the error of the missing data estimates (gray lines) are of the level of their predicted total uncertainty (noise and nonlinear distortion). The maximal error (first frequency excluded) on G_0 and G_1 is, respectively, -56.8 dB and -65.0 dB for the 20% clipping, and -58.2 dB and -63.1 dB for the 30% random pattern.

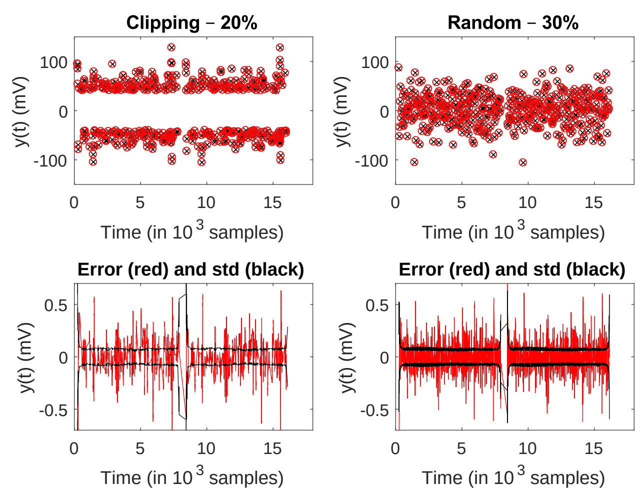

Figure 15. Comparison of the estimated and the true missing data. Top row (only one 1 out of 8 missing samples are shown): true (black x) and estimated (red o) samples – Measurement example. Bottom row (all missing samples are shown): difference between the true and estimated samples (red lines) and the predicted standard deviation (black lines). Left column: 30% randomly missing data (32 mVrms) with an estimation error of 0.14 mVrms. Right column: 20% clipping (58 mVrms) with an estimation error of 0.24 mVrms.

Figure 15 compares the estimated and the true missing data. It follows that the ratio of the rms value of the estimation error and the rms value of the missing samples is about 4×10^{-3} for both missing data patterns. This estimation error is mainly due to the nonlinear distortion (see Fig. 14, top left plot).

Since the true TV-FRF is unknown, the quality of the estimated TV-FRFs is verified in Fig. 16 by comparing the actual output DFT (no missing samples) to that predicted by

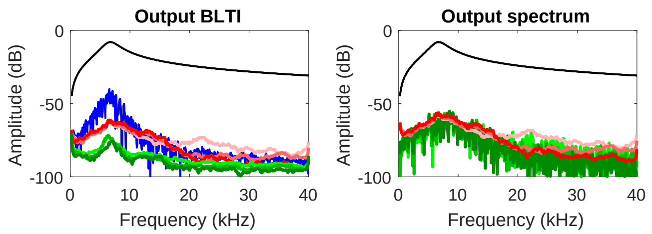

Figure 16. Left: split of the output DFT into the best linear time-invariant (BLTI) approximation (3 coinciding black lines), the noise variance (green lines), the total variance (red lines), and the time-varying effects (3 coinciding blue lines). Dark green and dark red: no missing data, medium green and medium red: 30% randomly missing data, and light green and light red: 20% clipping. Right: comparison of the measured to the simulated output DFT spectrum at the excited frequencies. Black lines: output DFT spectra (2 coinciding lines), green lines: simulation error, and red lines: total variance of the missing data estimates. Dark green and dark red lines: no missing data, medium green medium red: 30% randomly missing data, and light green and light red: 20% clipping.

the direct model (29) at the excited frequencies. From the right plot it can be seen that the estimation error (green lines) is at the level of its corresponding predicted total uncertainty (red lines), which validates the estimated direct models. Using the estimated direct models, the output DFT can be split into four contributions (see the left plot of Fig. 16): the best linear time-invariant part (black lines), the time-varying effect (blue lines), the noise variance (green lines), and the total variance (red lines).

C. Discussion

Although the weakly nonlinear, slowly time-varying electronic circuit does not satisfy Assumption 2, a finite value of N_b has been be found such that the bias error is smaller than the uncertainty due to the noise and the nonlinear distortion. Clipping is more sensitive to disturbing noise and nonlinear distortion. Indeed, for 30% clipping the maximal error on the G_0 and G_1 estimates increases from, respectively, -56.8 dB and -65.0 dB (see Fig. 14, right column) to, respectively, -53.3 dB and -55.2 dB, which is, respectively, 5 dB and 10 dB larger than that of the 30% random pattern. It illustrates the higher sensitivity to noise and nonlinear distortion of the clipping compared with the randomly missing pattern, which is in agreement with the observations in [32]. This is due to the removal of all extreme signal values in the clipping operation.

From the left plot of Fig. 16 one can easily decide whether the linear time-invariant framework is accurate enough for a given application or not, all of this in the presence of a large fraction of missing samples. If so, then it is sufficient to describe the dynamics by the best linear time-invariant approximation G_0 (Fig. 14, top left plot). However, if the time-varying effects (blue lines) are too large to be neglected, then the estimated direct model shown (Fig. 14) describes well the time-varying dynamics.

VIII. Conclusions

Using random phase multisine excitations it is possible to estimate nonparametrically the best linear time-invariant approximation of a particular class of nonlinear time-varying systems (see Assumption 2) in the presence of a large fraction (typically, 20%–30% for clipping and 30%–40% for a random pattern) of missing data, and to detect and quantify the noise level, the level of the nonlinear distortions, and the time-varying effects. As such the user can decide whether in a given application the linear time-invariant approximation of the true nonlinear time-varying dynamics is accurate enough or not.

If the time-varying effects are too important to be neglected (application dependent threshold), then the proposed approach provides the best linear time-varying approximation of a particular class of nonlinear time-varying systems together with its noise level and the level of the nonlinear distortions. As such the user can decide whether in a given application the linear time-varying approximation of the true nonlinear time-varying dynamics is accurate enough or not.

The simulation and experimental results indicate that the proposed estimation algorithm also performs well for nonlinear time-varying systems that do not exactly satisfy Assumption 2. For example, the relative estimation error of the missing samples (ratio rms values) is about 6×10^{-5} and 4×10^{-3} for, respectively, the simulations and the measurements. Although the method is applicable to almost any missing data pattern (random, clipping, burst of missing samples), the simulations and experiments reveal that some missing data patterns are more sensitive to the disturbing noise than others. Indeed, for the same missing data fraction, the maximal estimation error for clipping was observed to be 5 to 27 dB larger than that of the random pattern. The only drawback of the proposed method is that no missing samples are allowed at the borders of the excitation periods.

The Matlab software of the algorithm is available on demand.

Acknowledgments

This work is sponsored in part by the Research Council of the Vrije Universiteit Brussel (SRP 19), in part by the Research Foundation Flanders (FWO-Vlaanderen), and in part by the Flemish Government (Methusalem Fund METH1).

References

[1] L. Ljung, *System Identification: Theory for the User, second edition*. Upper Saddle River, New Jersey (US): Prentice-Hall, 1999.

[2] R. Pintelon, E. Louarroudi, and J. Lataire, "Time-variant frequency response function measurement on weakly nonlinear, arbitrarily time-varying systems excited by periodic inputs," *IEEE Trans. Instrum. and Meas.*, vol. 64, no. 10, pp. 2829-2837, Oct. 2015.

[3] D. Ugryumova, R. Pintelon, and G. Vandersteen, "Frequency response matrix estimation from partially missing data - for periodic inputs," *IEEE Trans. Instrum. Meas.*, vol. 64, no. 12, pp. 3615–3628, Dec. 2015.

[4] S. Y. Chen, and J. S. Yuan, "Adaptive gate bias for power amplifier temperature compensation," *IEEE Trans. on Device and Material Reliability*, vol. 11, no. 3, pp. 442-449, 2011.

[5] B. Bigland-Ritchie, "EMG/force relations and fatigue of human voluntary contractions," *Exercise and Sport Sciences Reviews*, vol. 9, no. 1, pp. 75-117, 1981.

[6] B. J. B. Grant, J. M. Fitzpatrick, and B. B. Lieber, "Time-varying pulmonary arterial compliance," *Journal of Applied Physiology*, vol. 70, no. 2, pp. 575-583, 1991.

[7] A. Jhinaoui, L. Mevel, and J. Morlier, “A new SSI algorithm for LPTV systems: Application to a hinged-bladed helicopter,” *Mechanical Systems and Signal Processing*, vol. 42, no. 1-2, pp. 152-166, 2014.

[8] R. P. Aguilera, B. I. Godoy, J. C. Agüero, G. C. Goodwin, and J. I. Yuz, “An EM-based identification algorithm for a class of hybrid systems with application to power electronics,” *International Journal of Control*, vol. 87, no. 7, pp. 1339-1351, 2014.

[9] S. Paoletti, A. Lj. Juloski, G. Ferrari-Trecate, and R. Vidal, “Identification of hybrid systems – A tutorial,” *European Journal of Control*, vol. 13, no. 2-3, pp. 242-260, 2007.

[10] B. F. Spencer, M. E. Ruiz-Sandoval and N. Kurata, “Smart sensing technology: opportunities and challenges,” *Struct. Control Health Monit.*, vol.11, no. 4, pp. 349–368, 2004.

[11] Y. Yang, and S. Nagarajaiah, “Harnessing data structure for recovery of randomly missing structural vibration responses time history: Sparse representation verus low-rank structure,” *Mech. Syst. and Sign. Proc.*, vol. 74, no. 1, pp. 165-182, 2016.

[12] R. Wallin, and A. Hansson “Maximum likelihood estimation of linear SISO models subject to missing output data and missing input data,” *Int. J. of Contr.*, vol. 87, no. 11, pp. 2354–2364, 2014.

[13] I. Markovsky, J. Goos, K. Usevich, and R. Pintelon, ”Realization and identification of autonomous linear periodically time-varying systems,” *Automatica*, vol. 50, no. 6, pp. 1632-1640, 2014.

[14] A. Hansson, and R. Wallin, “Maximum likelihood estimation of Gaussian models with missing data – Eight equivalent formulations,” *Automatica*, vol. 48, no. 9, pp. 1955-1962, 2012.

[15] R. Pintelon, D. Ugryumova, G. Vandersteen, E. Louarroudi, and J. Lataire, “Time-variant frequency response function measurement in the presence of missing data,” *IEEE Trans. Instrum. Meas.*, vol. 66, no. 11, pp. 3091–3099, Nov. 2017.

[16] J. Schoukens, G. Vandersteen, Y. Rolain, and R. Pintelon, “Frequency response function measurements using concatenated data records of arbitrary length,” *IEEE Trans. Instrum. and Meas.*, vol. 61, no. 10, pp. 2682-2688, 2012.

[17] K. Barbé, W. Van Moer, L. Lauwers, and N. Björsell, “A simple nonparametric preprocessing technique to correct for nonstationary effects in measured data,” *IEEE Trans. Instrum. and Meas.*, vol. 61, no. 8, pp. 2085–2094, 2012.

[18] L. A. Zadeh, “The determination of the impulsive response of variable networks,” *Journal of Applied Physics*, vol. 21, pp. 642–645, 1950.

[19] L. A. Zadeh, “Frequency analysis of variable networks,” *Proceedings of the I.R.E.*, vol. 38, pp. 291–299, 1950.

[20] B. Boashash, Ed., *Time Frequency Signal Analysis and Processing: A Comprehensive Reference*. Amsterdam, The Netherlands: Elsevier, 2003.

[21] M. Abramowitz, and I. A. Stegun*, Handbook of Mathematical Functions*. New York: Dover Publications, 1970.

[22] J. Lataire, E. Louarroudi, and R. Pintelon, “Detecting a time-varying behavior in frequency response function measurements,” *IEEE Trans. Instrum. and Meas.*, vol. 61, no. 8, pp. 2132–2143, 2012.

[23] J. Lataire, R. Pintelon, and E. Louarroudi, “Non-parametric estimate of the system function of a time-varying system,” *Automatica*, vol. 48, no. 4, pp. 666–672, 2012.

[24] R. Pintelon, E. Louarroudi, and J. Lataire, “Nonparametric time-variant frequency response function estimates using arbitrary excitations,” *Automatica*, vol. 51, no. 1, pp. 308–317, 2015.

[25] M. Enqvist, and L. Ljung, “Linear approximations of nonlinear FIR systems for separable input processes,” *Automatica*, vol. 41, no. 3, pp. 459–473, 2005.

[26] R. Pintelon, and J. Schoukens, *System Identification: A Frequency Domain Approach, second edition*. John Wiley–IEEE Press, Piscataway (USA), 2012.

[27] R. Pintelon, J. Schoukens, and P. Guillaume, “Continuous-time noise modelling from sampled data,” *IEEE Trans. Instrum. Meas.*, vol. 55, no. 6, pp. 2253–2258, June 2006.

[28] D. Ugryumova, R. Pintelon, and G. Vandersteen, “Frequency response function estimation in the presence of missing output data,” *IEEE Trans. Instrum. and Meas.*, vol. 64, no. 2, pp. 541–553, 2015.

[29] D. Ugryumova, R. Pintelon, and G. Vandersteen, “Frequency response matrix estimation from missing input-output data,” *IEEE Trans. Instrum. and Meas.*, vol. 64, no. 11, pp. 3124–3136, 2015.

[30] R. Pintelon, E. Louarroudi, and J. Lataire, “Time-variant frequency response function measurement of multivariate time-variant systems operating in feedback,” *IEEE Trans. Instrum. and Meas.*, vol. 66, no. 1, pp. 177-190, Jan. 2017.

[31] A. Ralston, and P. Rabinowitz, *A First Course in Numerical Analysis*. New York: McGraw-Hill, 1984.

[32] R. Pintelon, J. Lataire, G. Vandersteen, and D. Ugryumova, “Impact on the missing data pattern, the oversampling, the noise level, and the excitation on nonparametric frequency response function estimates,” *18th IFAC Symposium on System Identification, SYSID 2018*, Stockholm (Sweden), July 9–11, 2018.